

Dephasing in a quantum pump

J.N.H.J. Cremers,^a P.W. Brouwer^b

^a*Lyman Laboratory of Physics, Harvard University, Cambridge MA 02138*

^b*Laboratory of Atomic and Solid State Physics, Cornell University, Ithaca, NY 14853-2501*

(October 28, 2018)

We study how dephasing affects the distribution of the dc current pumped through a chaotic quantum dot. We introduce dephasing by the addition of a voltage probe to the quantum dot, treating both the case of controlled dephasing (when the voltage probe is coupled to the dot via a ballistic point contact with a conductance that is increased stepwise) and intrinsic dephasing (for which the voltage probe serves as a phenomenological model). While dephasing eventually suppresses the dc current through the dot, we also find that, for a quantum dot with single-mode point contacts, a small amount of dephasing actually decreases the likelihood of a zero pumped current.

PACS numbers: 72.10.Bg, 73.23.-b

I. INTRODUCTION

Quantum mechanical interference is a key player determining sample-specific properties of small metal or semiconductor particles. For closed systems, quantum interference fixes the precise positions of energy levels and the microscopic details of wavefunctions; for open systems it governs, e.g., the fluctuations of the conductance.^{1,2} In all these cases, interference provides a (sometimes large) correction added to a nonzero background. Such a background is absent in a so-called “quantum electron pump”, which has received considerable experimental³ and theoretical^{4–12} attention recently. This requirement of phase coherence for the observation of a pumped current makes a quantum pump a sensitive instrument to study quantum interference in quantum dots.

In the experimental proposal of Ref. 3, a quantum electron pump is made of a semiconductor quantum dot connected to two electron reservoirs. A dc current is generated by periodically varying two gate voltages that characterize shape of the dot. (Alternatively, one may pump electrons by periodic variation of the Fermi energy, magnetic flux, etc.) The electron pump is called “quantum”, because the variation pertains to the quantum interference only, not to the classical dynamics of the dot: In a trajectory-based picture, the variations affect phases of the trajectories, not their weights. For this reason, this “quantum” electron pump is fundamentally different from electron pumps or turnstiles that rely on Coulomb charging physics and do not require phase coherence.^{13,14} In the quantum pump, the precise value of the pumped current and its direction depend on microscopic details and vary from sample to sample. Therefore, one needs to address the probability distribution $P(I)$ of pumped currents for an ensemble of quantum pumps. Theoretical work has focused on electron pumps in a chaotic quantum dot, for which this distribution can be calculated using random matrix theory.^{5,6,8,10} For a pump with single-channel point contacts, it was found

that $P(I)$ has a cusp at $I = 0$ and algebraic tails,⁵ while for many-channel point contacts, $P(I)$ is Gaussian.^{5,6,8}

In this paper, we study how the probability distribution of the pumped current is affected if phase coherence in the quantum pump is gradually destroyed. As in Refs. 3,5–10, we consider the case of a quantum pump that consists of a chaotic quantum dot. A controlled way to destroy phase coherence is to couple the dot to a voltage probe.¹⁵ While not drawing a net current, the voltage probe absorbs and reinjects electrons without any phase-relationship, thereby destroying phase coherence. The dephasing rate γ_ϕ can be tuned by varying the conductance of the point contact connecting the quantum dot and the voltage probe. While a voltage probe can be used as an external source to controllably increase the dephasing rate in the quantum pump, it can also be used as a model for intrinsic dephasing processes in the pump itself, such as electron-electron interactions or two-level systems in the dot.^{15–17} A similar approach was taken in a recent paper by Moskalets and Büttiker, who studied the effect of a voltage probe on the current pumped through an electron pump consisting of a one-dimensional wire with two tunable tunnel barriers of oscillating strength.¹⁸ However, unlike the quantum dot geometry studied here, the pump of Ref. 18 can also operate as an electron pump in the absence of phase coherence. The variance of the pumped current in the case of many-channel point contacts was previously obtained by Shutenko *et al.* using a different model.⁸

In Sec. II we use the scattering approach to derive a formula for the pumped current in the presence of the voltage probe. In Sec. III we then study the distribution of the pumped current for the cases of controlled dephasing and intrinsic dephasing. We focus on the cases of a quantum dot with single channel point contacts and with multi-channel point contacts. We conclude in Sec. IV.

II. PUMPED CURRENT IN THE PRESENCE OF DEPHASING

A schematic picture of the system is shown in Fig.1. It consists of a quantum dot connected by ballistic point contacts to three electron reservoirs, labeled 1, 2, and 3. The point contacts allow N_1 , N_2 and N_3 propagating channels at the Fermi level, respectively. The total number of channels in all point contacts will be denoted as $N = N_1 + N_2 + N_3$. The reservoirs 1 and 2 are held at the same voltage $V_1 = V_2 = 0$, while reservoir 3 serves as a voltage probe: the time-dependent voltage $V_3(t)$ is adjusted such that the current $I_3(t) = 0$ at all times.

Two external parameters $X_1(t)$ and $X_2(t)$ that determine the shape (or other characteristics) of the quantum dot are varied periodically with frequency ω . As a result of this periodic variation, a dc current $I = I_1 = -I_2$ will flow between reservoirs 1 and 2. We will now evaluate this pumped current in the presence of the voltage probe. Starting point of our evaluation is the relation⁵ between the pumped current and the emissivity $edn(m)/dX_j$, the charge that leaves the dot through contact $m = 1, 2$ as the parameter X_j is varied by an amount dX_j ,

$$I = \frac{\omega e}{2\pi} \int_A dX_1 dX_2 \left[\frac{\partial}{\partial X_1} \left(\frac{dn(1)}{dX_2} \right) - \frac{\partial}{\partial X_2} \left(\frac{dn(1)}{dX_1} \right) \right]. \quad (1)$$

Here A is the area in (X_1, X_2) -space enclosed by the parameters $[X_1(t), X_2(t)]$ in one cycle. Equation (1) is valid for the adiabatic regime, $\omega\tau_d \ll 1$, where $\tau_d \sim \hbar/N\Delta$ is the dwell time of the quantum dot, Δ being the mean single-particle level spacing.

In the absence of the voltage probe, and for ballistic point contacts between the dot and reservoirs 1 and 2, so that effects of charge quantization in the dot can be ignored,¹⁹ the emissivity $edn(m)/dX_j$ is related to the $N \times N$ scattering matrix S of the dot as²⁰

$$\frac{dn(m)}{dX} = \frac{1}{2\pi} \sum_{\beta} \sum_{\alpha \in m} \text{Im} \frac{\partial S_{\alpha\beta}}{\partial X} S_{\alpha\beta}^*. \quad (2)$$

With voltage probe, charge can either leave the quantum dot directly through the contacts 1 or 2, or via inelastic scattering in reservoir 3. Hence, we can write the emissivity $dn(m)/dX$ as a sum of an elastic and an inelastic contribution,

$$\frac{dn(m)}{dX} = \left(\frac{dn(m)}{dX} \right)_{\text{el}} + \left(\frac{dn(m)}{dX} \right)_{\text{in}}, \quad (3)$$

where the elastic contribution $(dn(m)/dX)_{\text{el}}$ is still given by Eq. (2) and the inelastic contribution reads

$$\left(\frac{dn(m)}{dX} \right)_{\text{in}} = \frac{G_{m3}}{2\pi(G_{13} + G_{23})} \text{Im} \sum_{\beta} \sum_{\alpha \in 3} \frac{\partial S_{\alpha\beta}}{\partial X} S_{\alpha\beta}^*. \quad (4)$$

Here

$$G_{ij} = \sum_{\alpha \in i} \sum_{\beta \in j} |S_{\alpha\beta}|^2$$

is an element of the 3×3 conductance matrix of the dot. Substitution of Eqs. (2)–(4) into Eq. (1) then yields the current formula

$$I = \frac{\omega e}{2\pi} \int_A dX_1 dX_2 (i_{\text{dir}} + i_{\text{rect}}), \quad (5a)$$

$$i_{\text{dir}} = \frac{G_{23}}{\pi(G_{13} + G_{23})} \text{Im} \sum_{\beta} \sum_{\alpha \in 1} \frac{\partial S_{\alpha\beta}}{\partial X_2} \frac{\partial S_{\alpha\beta}^*}{\partial X_1} - \frac{G_{13}}{\pi(G_{13} + G_{23})} \text{Im} \sum_{\beta} \sum_{\alpha \in 2} \frac{\partial S_{\alpha\beta}}{\partial X_2} \frac{\partial S_{\alpha\beta}^*}{\partial X_1}, \quad (5b)$$

$$i_{\text{rect}} = \frac{1}{4\pi} \text{Im} \sum_{\beta} \sum_{\alpha \in 3} S_{\alpha\beta}^* \frac{\partial S_{\alpha\beta}}{\partial X_2} \frac{\partial}{\partial X_1} \frac{G_{13} - G_{23}}{G_{13} + G_{23}} - \frac{1}{4\pi} \text{Im} \sum_{\beta} \sum_{\alpha \in 3} S_{\alpha\beta}^* \frac{\partial S_{\alpha\beta}}{\partial X_1} \frac{\partial}{\partial X_2} \frac{G_{13} - G_{23}}{G_{13} + G_{23}}. \quad (5c)$$

The first contribution I_{dir} represents the charge that exits the dot either directly or indirectly via the reservoir, while the second contribution I_{rect} is an additional contribution to the dc current that arises from rectification of the voltage $V_3(t)$.¹⁸ One verifies that in the limit where the third reservoir is decoupled from the quantum dot, I_{rect} vanishes, while the expression for I_{dir} approaches that for current in the absence of dephasing (see Ref. 5).

In the next section we proceed to calculate the statistical distribution of the current I for an ensemble of chaotic quantum dots. We restrict ourselves to the case of small pumping amplitudes $X_1 = \delta X_1 \sin(\omega t)$, $X_2 = \delta X_2 \sin(\omega t + \phi)$, for which the current I is bilinear in δX_1 and δX_2 ,

$$I = \frac{1}{2} e \omega i \sin \phi \delta X_1 \delta X_2, \quad i = i_{\text{dir}} + i_{\text{rect}}. \quad (6)$$

We will consider both the case of “controlled dephasing”, corresponding to a real voltage probe coupled to the quantum dot via a ballistic point contact, and that of intrinsic dephasing, which is modeled by a voltage probe coupled to the quantum dot via a wide tunneling contact.¹⁷

In the absence of dephasing, the pumped current is not symmetric under reversal of a magnetic field through the quantum dot.^{8,11} One easily verifies that in the presence of dephasing the current I remains asymmetric under reversal of the magnetic field, even in the presence of strong dephasing (N_3 large).

III. DISTRIBUTION OF THE PUMPED CURRENT IN THE PRESENCE OF DEPHASING

For an ensemble of chaotic quantum dots the distribution of the scattering matrix and its derivatives is

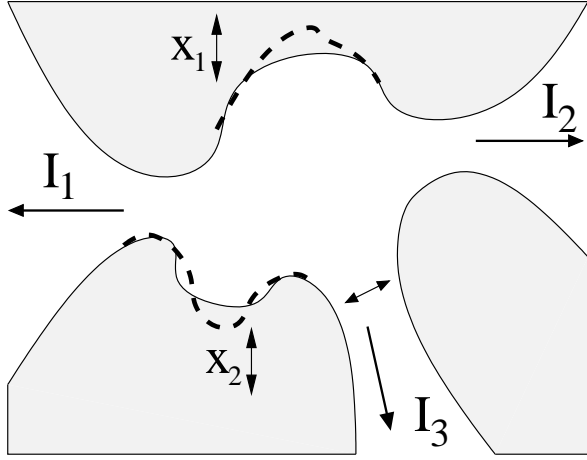


FIG. 1. A quantum dot with two parameters X_1 and X_2 which describe a deformation of its shape. As X_1 and X_2 are varied periodically a dc current $I = I_1 = -I_2$ flows from the right to the left reservoir. The lead on the bottom, through which no current flows ($I_3 = 0$), has a variable number of channels N_3 .

known.²¹ It is most conveniently expressed through the parameterization

$$S = UU', \quad \frac{\partial S}{\partial X_j} = UQ_jU', \quad (7)$$

where U and U' are $N \times N$ unitary matrices and Q_j is an $N \times N$ hermitian matrix. In the presence of time-reversal symmetry, $U' = U^T$ and $Q_j = Q_j^T$. We also introduce the matrix Q_ε that parameterizes the energy-derivative $\partial S/\partial \varepsilon$,

$$\frac{\partial S}{\partial \varepsilon} = \frac{2\pi}{\Delta} UQ_\varepsilon U'.$$

For ballistic point contacts to reservoirs 1, 2, and 3, the matrices U and U' are uniformly distributed in the unitary group, independently of Q_1 , Q_2 , and Q_ε , while the joint distribution of the matrices Q_1 , Q_2 , and Q_ε is given by

$$P \propto (\det Q_\varepsilon)^{-N/2-2(\beta N+2-\beta)} \Theta(Q) \times \exp \left[-\frac{\beta}{2} \text{tr} \left(Q_\varepsilon^{-1} + \frac{1}{8} \sum_{j=1}^2 (Q_\varepsilon^{-1} Q_j)^2 \right) \right], \quad (8)$$

where $\Theta(Q) = 1$ if all eigenvalues of Q are positive and $\Theta(Q) = 0$ otherwise and $\beta = 1$ (2) in the presence (absence) of time-reversal symmetry. Note that at fixed Q_ε the distribution of Q_1 and Q_2 is Gaussian with a width set by Q_ε .

We will now study the distribution of the pumped dc current for controlled dephasing and intrinsic dephasing. In each case we will first study the variance and then the full distribution.

A. Controlled Dephasing

The effect of dephasing on the distribution of the pumped current can be studied in a controlled setting by increasing the number N_3 of open channels in the voltage probe one by one. The third reservoir serves as a true voltage probe if the charge relaxation rate of that reservoir is much larger than the frequency ω , so that the voltage $V_3(t)$ can adjust essentially instantaneously to balance any current $I_3(t)$ flowing into or out of that reservoir as a result of the pumping action on the quantum dot.

A voltage probe connected to the dot via a ballistic point contact with N_3 channels gives rise to a dephasing rate

$$\gamma_\phi = \frac{1}{\tau_\phi} = N_3 \Delta / h. \quad (9)$$

We now fix N_1 and N_2 and calculate the distribution of the pumped current as a function of N_3 . We consider the cases $N_1 = N_2 = 1$ of single channel current-carrying leads and $N_1, N_2 \gg 1$ of many-channel current-carrying leads. In the former case, we have calculated the first two moments of the distribution $P(i)$ of the dimensionless current i analytically, using the technique of Ref. 22 to perform the integrations over the matrices U and U' . The average current $\langle i \rangle$ was thus found to be zero, while the variance $\langle i^2 \rangle$ decreases with increasing N_3 ; $\langle i^2 \rangle$ is divergent for $N_3 = 0$ for $\beta = 2$ and for $N_3 < 6$ for $\beta = 1$. The results of this calculation are shown in Fig. 2. For large N_3 , we find

$$\langle i^2 \rangle = \langle i_{\text{dir}}^2 \rangle = \frac{16N_1N_2}{\pi^2(N_1 + N_2)(N_1 + N_2 + N_3)^3}. \quad (10)$$

Details of the calculation can be found in Appendix A. [Equation (10) is valid for arbitrary N_1 and N_2 , as long as $N_3 \gg 1$.] For $N_3 \gg 1$, the contribution of the rectification current i_{rect} to $\langle i^2 \rangle$ is proportional to N_3^{-4} and hence negligible. (A similar conclusion for the rectification contribution was reached in Ref. 12 for the comparison of measurements of pumped current and pumped voltage.) As shown in Fig. 2, in general, $\langle i^2 \rangle$ is larger with time-reversal symmetry than without, though the difference between the two variances vanishes for large dephasing rates.

We obtained the full distribution $P(i)$ for $N_1 = N_2 = 1$ using Monte-Carlo integration with the distribution (8). The result is shown in Fig. 3 for various values of N_3 . Details of the numerical procedure are outlined in App. B. Note that the distributions are symmetric around $i = 0$. In the absence of dephasing ($N_3 = 0$), $P(i)$ has a cusp at $i = 0$, which is smoothed out for $N_3 > 0$. The distribution $P(i)$ has algebraic tails with powers that increase with increasing dephasing rate. In the presence of time-reversal symmetry the tails fall off with a power smaller than 3 as long as $N_3 < 6$, corresponding to a divergent second moment $\langle i^2 \rangle$ (cf. Fig. 2). Interestingly, while

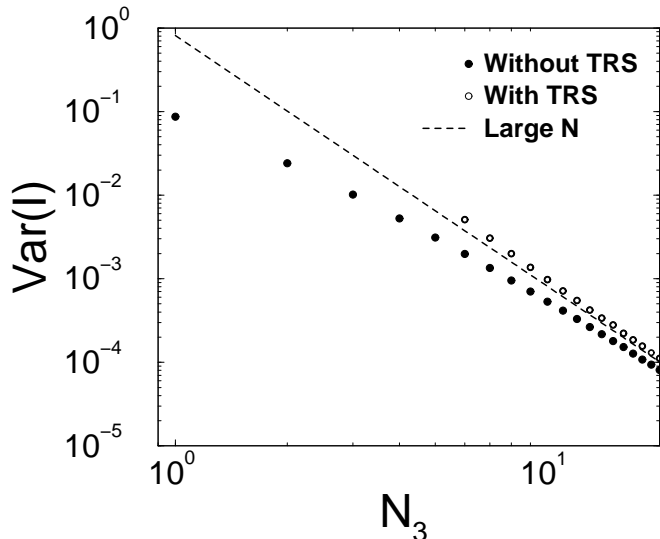


FIG. 2. Variance of the pumped current with one open channel in each of the current carrying leads ($N_1 = N_2 = 1$) as a function of the number of open channels in the third lead (N_3). The presence (absence) of time-reversal symmetry is denoted by open circles (closed circles). The dashed line is the variance in the asymptotic limit $N_1 = N_2 = 1$, $N_3 \rightarrow \infty$. The variance in the presence of time-reversal symmetry is infinite for $N_3 < 6$.

dephasing decreases the second moment $\langle i^2 \rangle$ for single-channel point contacts $N_1 = N_2 = 1$, a small amount of dephasing also decreases the probability $P(i = 0)$ of finding no pumped current at all. This can be understood physically, since the cusp in the distribution $P(i)$ at zero pumped current arises from the occurrence of destructive interference, which is as much suppressed by dephasing as the constructive interference responsible for large values of i and the tails of the distribution. For $N_3 \gg 1$, the distribution $P(i)$ approaches a Gaussian.

For multichannel point contacts in the current-carrying leads, $N_1, N_2 \gg 1$, the distribution $P(i)$ is a Gaussian centered around $i = 0$. To calculate the second moment $\langle i^2 \rangle$, we parameterize the scattering matrix S and its derivatives as in Eq. (7), perform the Gaussian integration over Q_1 and Q_2 with the distribution (8) at fixed Q_ε , integrate over the unitary matrices U and U' using the diagrammatic technique of Ref. 22 and finally integrate over the eigenvalues τ_j , $j = 1, \dots, N$, of Q_ε , see appendix A for details. The result is given by Eq. (10) above.

B. Intrinsic dephasing

The voltage probe can also be used as a model for intrinsic dephasing in the quantum dot. Sources of dephasing may be, e.g., electron-electron interactions or interactions with an external bath of photons and/or phonons. In such a case the source of decoherence is delocalized

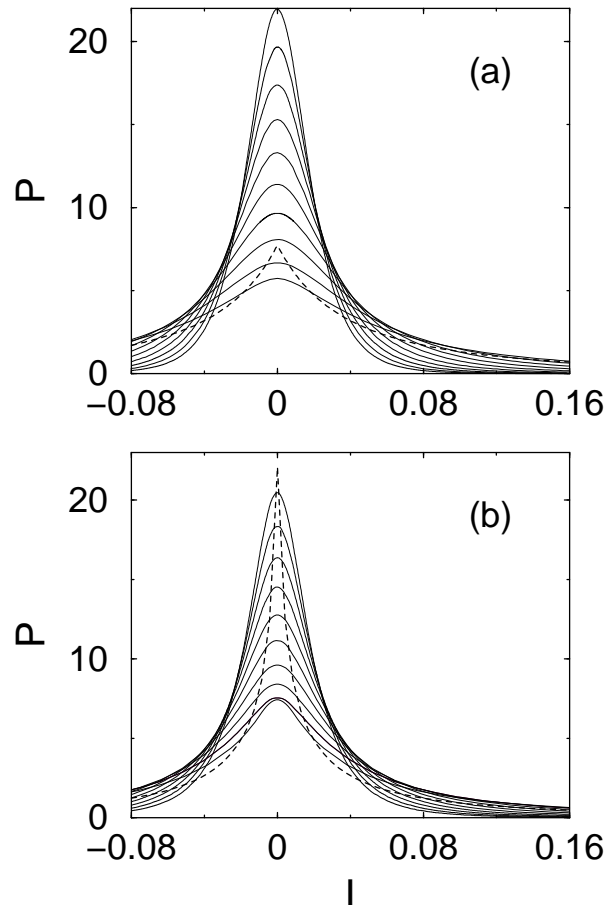


FIG. 3. The probability distribution of the pumped current without (a) and with (b) time-reversal symmetry, for the case $N_1 = N_2 = 1$ of single-channel point contacts in the current-carrying leads and as a function of the number of channels N_3 in the voltage probe. The dashed line shows the distribution without dephasing ($N_3 = 0$). The solid lines show the distribution with $N_3 = 1$, (lowest curve at $i = 0$) 2, ..., $N_3 = 10$ (highest curve).

throughout the dot. This situation is well modeled by a voltage probe with a tunnel barrier with transmission probability $\Gamma_3 \ll 1$ and many channels $N_3 \gg 1$, such that the product

$$N_3\Gamma_3 = \frac{h\gamma\phi}{\Delta} \quad (11)$$

is kept fixed.¹⁷

In order to find the distribution of the pumped current in this case, we need the distribution of the scattering matrix S and its derivatives when the contact to the third reservoir contains a tunnel barrier. This problem can be solved by a statistical mapping which connects the scattering matrix S to a scattering matrix S_0 that is taken from an ensemble appropriate for a quantum dot with ballistic point contacts,^{23,24}

$$S = \sqrt{1-\Gamma} - \sqrt{\Gamma} \frac{1}{1 - S_0\sqrt{1-\Gamma}} S_0 \sqrt{\Gamma}, \quad (12)$$

where Γ is a diagonal $N \times N$ matrix with $\Gamma_{jj} = 0$ for index j corresponding to the current-carrying leads 1 and 2 and $\Gamma_{jj} = \Gamma_3$ for index j corresponding to the voltage probe. The distribution of S_0 and its derivatives is as described in Eqs. (7)–(8) at the beginning of this section. We can then find the distribution of S from Eq. (12) and the distribution of its derivatives upon differentiating Eq. (12).

We have calculated the variance $\langle i^2 \rangle$ and the full distribution of the current for $N_1 = N_2 = 1$ using Monte-Carlo integration with the above distribution. The results are shown in Figs. 4 and 5. We note that intrinsic dephasing cuts off the tails of the distribution $P(i)$. This is in contrast to the case of controlled dephasing by a few-channel voltage probe with ballistic point contacts, which merely replaces the algebraic tail of the distribution at zero dephasing by another, faster decaying, algebraic tail. As for controlled dephasing, the variance of the pumped current is larger with time-reversal symmetry than without, though for intrinsic dephasing the difference is smaller than in the case of controlled dephasing (cf. Fig. 2). At large dephasing rates, the dependence of $\langle i^2 \rangle$ on the presence or absence of time-reversal symmetry vanishes. Also note that the probability to find zero pumped current initially decreases when the dephasing rate is increased, although the effect is not as strong as in the case of controlled dephasing. For large dephasing rates, both intrinsic and controlled dephasing yield the same distribution $P(i)$.

For large N_1 and N_2 the distribution $P(i)$ is again Gaussian, with zero mean and with variance given by Eq. (10) above with N_3 replaced by γ . This result agrees with what was previously obtained by Shutenko *et al.* using a different method.⁸

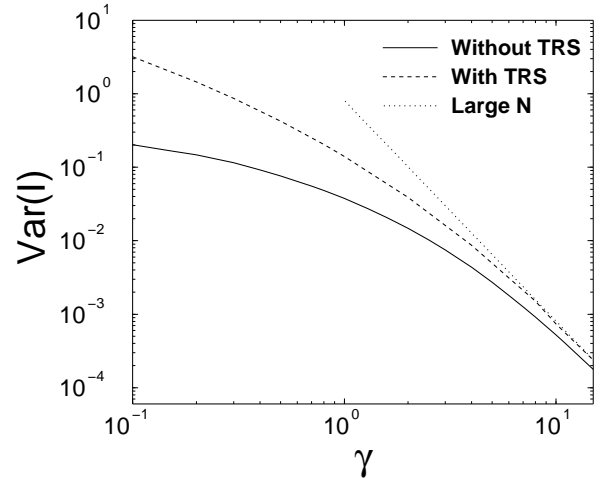


FIG. 4. The variance of the pumped current in the case of intrinsic dephasing as a function of dimensionless dephasing rate γ in the presence (dashed curve) and absence (solid curve) of time-reversal symmetry. The asymptotic result (dotted curve) is also shown. There is one open channel in each lead ($N_1 = N_2 = 1$).

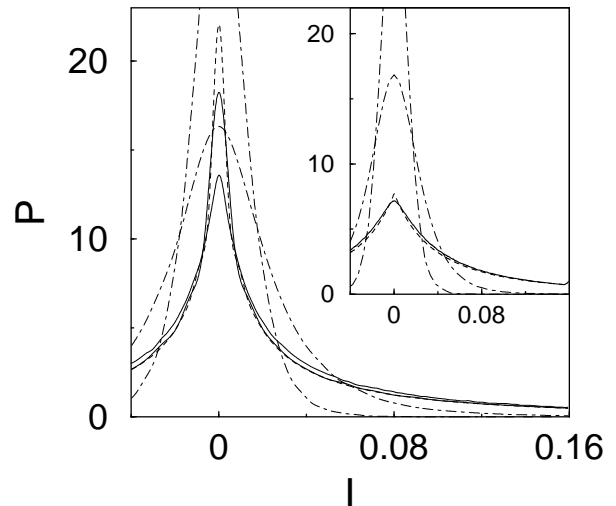


FIG. 5. The probability distribution of the pumped current with $N_1 = N_2 = 1$ in the presence of time-reversal symmetry and intrinsic dephasing. The dashed curve is the probability distribution in the absence of dephasing. The two solid curves have dimensionless dephasing rates $\gamma = .1$ (highest) and $\gamma = 1$ (lowest). The dot-dashed curves have dephasing rates $\gamma = 8$ (lowest) and $\gamma = 15$ (highest). The inset shows the probability distribution of the pumped current with $N_1 = N_2 = 1$ in the absence of time-reversal symmetry with the same parameters. The distribution with $\gamma = .1$ is indistinguishable from the case without dephasing ($\gamma = 0$).

IV. CONCLUSION

In summary, we have derived the current distribution of electrons pumped adiabatically through a chaotic quantum dot, in the presence of a voltage probe. The voltage can either serve as a controlled source of dephasing, or as an effective description of intrinsic dephasing processes inside the quantum dot. For the case of a quantum dot with two single-mode current-carrying point contacts, the conductance distribution is non-Gaussian with algebraic tails. Remarkably, while dephasing shifts the weight of the probability distribution $P(I)$ of the pumped current towards zero current, a small amount of dephasing actually reduces the probability $P(I = 0)$ to find no pumped current at all. This can be understood if the probability to find zero pumped current is enhanced by destructive interference — note the cusp in $P(I)$ at $I = 0$ —, which is then suppressed by dephasing. For a quantum dot with many-channel point contacts (as well as for a quantum dot with single-channel point contacts and a large dephasing rate), the current distribution is Gaussian. The width of the distribution decreases monotonically with increasing dephasing rate. For dephasing rates γ_ϕ much larger than the escape rate $\gamma \sim (N_1 + N_2)\Delta$ to the reservoirs, the r.m.s. current decays $\propto (\gamma/\gamma_\phi)^{3/2}$ (see also Ref. 8).

Not only dephasing, but also thermal smearing can reduce the size of the pumped current. Thermal smearing has been considered by Shutenko *et al.*,⁸ who found that, without dephasing, the r.m.s. current decays $\propto (\gamma/T)^{-1/2}$ for temperature $T \gg \gamma$. Experimentally, the dephasing rate γ_ϕ has been found to increase $\propto T$ (or faster), which implies that, for such a dephasing rate, dephasing is the more effective mechanism to reduce the current pumped in a quantum pump.

It is interesting to compare the quantum pump to a (quantum) rectifier. The latter device generates a dc current in response to an a.c. bias voltage. For a setup similar to the quantum dot pump considered here, the variance of the rectified current is proportional to $(\partial G/\partial X)^2$.²⁵ For large dephasing rates, typically $(\partial G/\partial X)^2 \sim (\gamma/\gamma_\phi)^3$,²⁶ so that the r.m.s. rectified current decays $\propto (\gamma/\gamma_\phi)^{3/2}$. As in an experimental realization a true quantum pump may coexist with a rectifier (the a.c. voltages arising from displacement currents and parasitic capacitive coupling),²⁷ we conclude that dephasing does not change the relative importance of one mechanism over the other.

ACKNOWLEDGMENTS

We thank B.I. Halperin and C. Marcus for stimulating discussions. Shortly before completion of our manuscript, we learned of Ref. 18, where the effect of dephasing in an electron pump is studied with an approach similar to ours. This work was supported by the NSF under grant

nos. DMR 0086509 and DMR 9981283 and by the Sloan foundation.

APPENDIX A:

In this appendix we outline the calculation of the moments $\langle i^2 \rangle$ in the presence of controlled dephasing. A detailed report of the calculations will appear in Ref. 29.

In order to calculate the average $\langle i^2 \rangle$, we need to perform an average over the $N \times N$ matrices U , U' , Q_1 , and Q_2 defined in Eq. (7). The matrices U and U' are uniformly distributed in the unitary group [$U' = U^T$ in the presence of time-reversal symmetry (TRS)], while the distribution of the matrices Q_1 and Q_2 is given by Eq. (8). First we perform the average over Q_1 and Q_2 . Hereto, we parameterize Q_1 and Q_2 as

$$Q_i = \Psi^{\dagger-1} H_i \Psi^{-1}, \quad i = 1, 2, \quad (\text{A1})$$

where H_1 and H_2 are hermitian $N \times N$ matrices (real symmetric in the presence of time-reversal symmetry) and Ψ is a complex (real) $N \times N$ matrix such that²⁸

$$Q_\varepsilon = \Psi^{\dagger-1} \Psi^{-1}. \quad (\text{A2})$$

Substitution of Eqs. (A1) and (A2) into the distribution (8) shows that the elements of H_1 and H_2 have a Gaussian distribution with zero mean and with variance

$$\langle H_{ij} H_{kl} \rangle = \begin{cases} 4 (\delta_{il} \delta_{jk} + \delta_{ik} \delta_{jl}) & \text{TRS,} \\ 4 \delta_{il} \delta_{jk} & \text{no TRS.} \end{cases} \quad (\text{A3})$$

We first perform the Gaussian average over the matrices H_1 and H_2 . The resulting expression contains the matrix Ψ in the combination $Q_\varepsilon = \Psi^{\dagger-1} \Psi^{-1}$ only. We decompose Q_ε in terms of its eigenvalue matrix $\hat{\tau}$ and a random unitary (orthogonal) matrix V ,

$$Q_\varepsilon = V \hat{\tau} V^\dagger. \quad (\text{A4})$$

and average over V using the diagrammatic method of Ref. 22 (or its straightforward generalization to orthogonal matrices V in the case when time-reversal symmetry is present). The result of the average is an expression that depends on the scattering matrix S and the matrix of eigenvalues $\hat{\tau}$ only.

In the absence of time-reversal symmetry, the result of this calculation is

$$\langle i_{\text{dir}}^2 \rangle = \frac{8}{\pi^2 N(N^2 - 1)} (\text{tr } \hat{\tau}^2 (\text{tr } \hat{\tau})^2 - \text{tr } \hat{\tau}^4) \times \left(N_1 N_2 + N_3 \frac{N_1 G_{23}^2 + N_2 G_{13}^2}{(G_{13} + G_{23})^2} \right) \quad (\text{A5})$$

while in the presence of time-reversal symmetry, we find

$$\langle i_{\text{dir}}^2 \rangle = \frac{8}{\pi^2 N(N - 1)} \left(G_{12} + \frac{G_{13} G_{23}}{G_{13} + G_{23}} \right) (\text{tr } \hat{\tau}^2 (\text{tr } \hat{\tau})^2 - (\text{tr } \hat{\tau}^2)^2 + 2 \text{tr } \hat{\tau} (\text{tr } \hat{\tau}^3) - 2 \text{tr } \hat{\tau}^4). \quad (\text{A6})$$

The contribution from i_{rect} is a factor N smaller than i_{dir} for large N . Now, the large- N result, Eq. (10), follows easily employing the known density of dimensionless delay times,

$$\begin{aligned} \rho(\tau) &= \left\langle \sum_j \delta(\tau - \tau_j) \right\rangle \\ &= \frac{N}{2\pi\tau^2} \sqrt{(\tau_+ - \tau)(\tau - \tau_-)}, \end{aligned} \quad (\text{A7})$$

where $\tau_{\pm} = (3 \pm \sqrt{8})/N$, to integrate over $\hat{\tau}$.

For the case $N_1 = N_2 = 1$, we were able to obtain exact expressions for $\langle i_{\text{dir}} i_{\text{rect}} \rangle$ and $\langle i_{\text{rect}}^2 \rangle$ for arbitrary N_3 and time-reversal symmetry is broken. These expressions, which contain up to a product of four traces involving the matrix $\hat{\tau}$, were too lengthy to be reported here, and will be published in Ref. 29. The results for $\langle i^2 \rangle$ are shown in Fig. 2. We summarize the main steps of the calculation below. Starting from Eq. (A5) and similar expressions for the variance of i_{rect} ,²⁹ we integrate over the eigenvalues τ_j of the dimensionless time-delay matrix Q_ε and the scattering matrix S . To average over the τ_j , $j = 1, \dots, N$, we introduce the dimensionless escape rates $x_n = 1/\tau_n$ which are distributed according to the generalized Laguerre ensemble,²¹

$$P(x_1, \dots, x_N) \propto \prod_{n < m} (x_n - x_m)^2 \prod_n x_n^N \exp(x_n). \quad (\text{A8})$$

Since the τ_n appear only in products of up to four traces, we need the marginal n -point distributions $R_n(x_1, \dots, x_n)$ for $n = 1, \dots, 4$ only, where

$$\begin{aligned} R_n(x_1, \dots, x_n) &= \frac{N!}{(N-n)!} \\ &\times \int_0^\infty dx_{n+1} \dots dx_N P(x_1, \dots, x_N). \end{aligned}$$

We can find exact expressions of R_1, \dots, R_4 using the associated Laguerre polynomials $L_n^N(x)$ which are orthogonal with respect to the weight function $x^N e^{-x}$. In particular, for the case of broken time-reversal symmetry,

$$R_n(x_1, \dots, x_n) = \det [K(x_i, x_j)]_{i,j=1,\dots,n},$$

where

$$K(x_i, x_j) = \sum_{l=1}^N L_l^N(x_i) L_l^N(x_j) e^{(x_i+x_j)/2} (x_i x_j)^{N/2}.$$

The average over S can be done using the polar decomposition of S ,

$$S = \begin{pmatrix} u & 0 \\ 0 & v \end{pmatrix} \begin{pmatrix} \sqrt{1-t^\dagger t} & it^\dagger \\ it & \sqrt{1-t^\dagger t} \end{pmatrix} \begin{pmatrix} u' & 0 \\ 0 & v' \end{pmatrix},$$

where u and u' (v and v') are 2×2 ($N_3 \times N_3$) unitary matrices and t is an $N_3 \times 2$ matrix with all elements equal

to zero except $t_{nn} = \sqrt{T_n}$, $n = 1, 2$. In the presence of time-reversal symmetry, $u' = u^T$ and $v' = v^T$. The parameters T_1 and T_2 govern the escape rate into the voltage probe. The uniform distribution of U and U' in the unitary group yields the integration measure

$$dS = |T_1 - T_2|^2 (T_1 T_2)^{N_3-2} du du' dv dv' dT_1 dT_2.$$

The average over S then reduces to an integral over T_1, T_2 and one angle ϕ uniformly distributed in the interval $0 < \phi < \pi/2$. In terms of these variables we can write

$$\begin{aligned} G_{13} &= T_1 \cos^2 \phi + T_2 \sin^2 \phi \\ G_{23} &= T_1 \sin^2 \phi + T_2 \cos^2 \phi \\ \text{tr } S_{33} S_{33}^\dagger S_{33} S_{33}^\dagger &= N - 4 + (1 - T_1)^2 + (1 - T_2)^2 \\ \text{tr } S_{13}^\dagger S_{13} S_{33}^\dagger S_{33} &= (1 - T_1) T_1 \cos^2 \phi + (1 - T_2) T_2 \sin^2 \phi, \end{aligned}$$

where S_{ij} denotes the ij block in the scattering matrix S . (The last two terms appear in the expression for i_{rect} .²⁹)

APPENDIX B:

In order to obtain the full distribution of the pumped current i , we numerically generated matrices U, U', Q_1 , and Q_2 according to the appropriate distributions. The matrices U and U' are uniformly distributed in the unitary group ($U' = U^T$ in the presence of time-reversal symmetry). Using a parameterization in terms of Euler angles,³⁰ their generation is relatively straightforward. The numerical generation of matrices Q_1 and Q_2 according to the distribution (8) makes use of a trick that was inspired by Ref. 31, which would like to explain below.

We parameterize the $N \times N$ matrices Q_1, Q_2 , and Q_ε as

$$\begin{aligned} Q_\varepsilon &= C^{\text{T}-1} C^{-1}, \\ Q_i &= C^{\text{T}-1} H_i C^{-1}, \quad i = 1, 2 \end{aligned} \quad (\text{B1})$$

where C is a complex $N \times 2N$ matrix [real $N \times (2N+1)$ matrix in the presence of time-reversal symmetry] and H_i ($i = 1, 2$) is a hermitian $2N \times 2N$ matrix [real symmetric $(2N+1) \times (2N+1)$ matrix in the presence of time-reversal symmetry]. In Eq. (B1), the inverse C^{-1} is defined as the right-inverse, $C^{-1} = C^T (C C^T)^{-1}$. In Ref. 31 it was shown that the matrix Q_ε has the distribution (8) if the elements of C are all chosen from a Gaussian distribution with unit variance. From there, one can show by substitution of Eq. (B1) into Eq. (8), that the parameterization (B1) reproduces the correct distribution (8) for all three matrices Q_ε, Q_1 , and Q_2 if the elements of the matrices H_1 and H_2 are all chosen from a Gaussian distribution with variance given by Eq. (A3) above.

- ¹ *Mesoscopic Quantum Physics*, edited by E. Akkermans, G. Montambaux, J.-L. Pichard, and J. Zinn-Justin (North-Holland, Amsterdam, 1995).
- ² L. P. Kouwenhoven, C. M. Marcus, P. L. McEuen, S. Tarucha, R. M. Westervelt, and N. S. Wingreen, in *Mesoscopic Electron Transport*, edited by L. L. Sohn, L. P. Kouwenhoven, and G. Schön (Kluwer, Dordrecht, 1997).
- ³ M. Switkes, C. M. Marcus, K. Campman, and A. C. Gos-sard, *Science* **283**, 1905 (1999).
- ⁴ B. Spivak, F. Zhou, and M. T. Beal Monod, *Phys. Rev. B* **51**, 13226 (1995).
- ⁵ P. W. Brouwer, *Phys. Rev. B* **58**, 10135 (1998).
- ⁶ F. Zhou, B. Spivak, and B. L. Altshuler, *Phys. Rev. Lett.* **82**, 608 (1999).
- ⁷ B. L. Altshuler and L. I. Glazman, *Science* **283**, 1864 (1999).
- ⁸ T. A. Shutenko, I. L. Aleiner, and B. L. Altshuler, *Phys. Rev. B* **61**, 10366 (2000).
- ⁹ J. E. Avron, A. Elgart, G. M. Graf, and L. Sadun, *Phys. Rev. B* **62**, 10618 (2000).
- ¹⁰ M. G. Vavilov, V. Ambegaokar and I. L. Aleiner, *Phys. Rev. B* **63**, 195313 (2001).
- ¹¹ I. L. Aleiner, B. L. Altshuler, and A. Kamenev, *Phys. Rev. B* **62**, 10373 (2000).
- ¹² M. L. Polianski and P. W. Brouwer, *Phys. Rev. B* **64**, 75304 (2001).
- ¹³ L. P. Kouwenhoven, A. T. Johnson, N. C. van der Vaart, C. J. P. M. Harmans, and C. T. Foxon, *Phys. Rev. Lett.* **67**, 1626 (1991).
- ¹⁴ H. Pothier, P. Lafarge, C. Urbina, D. Esteve, and M. H. Devoret, *Europhys. Lett.* **17**, 249 (1992).
- ¹⁵ M. Büttiker, *Phys. Rev. B* **33**, 3020 (1986); *IBM J. Res. Dev.* **32**, 63 (1988).
- ¹⁶ H. U. Baranger and P. A. Mello, *Phys. Rev. B* **51**, 4703 (1995).
- ¹⁷ P. W. Brouwer and C. W. J. Beenakker, *Phys. Rev. B* **55**, 4695 (1997).
- ¹⁸ M. Moskalets and M. Büttiker, cond-mat/0108061.
- ¹⁹ I. L. Aleiner, P. W. Brouwer, and L. I. Glazman, cond-mat/0103008.
- ²⁰ M. Büttiker, *J. Phys. Condens. Matter* **5**, 9361 (1993); M. Büttiker, H. Thomas, and A. Prêtre, *Z. Phys. B* **94**, 133 (1994).
- ²¹ P. W. Brouwer, K. M. Frahm, and C. W. J. Beenakker, *Phys. Rev. Lett.* **78**, 4737 (1997); *Waves in Random Media* **9**, 91 (1999).
- ²² P. W. Brouwer and C. W. J. Beenakker, *J. Math. Phys.* **37**, 4904 (1996).
- ²³ P. A. Mello, P. Pereyra and T. H. Seligman, *Ann. Phys.* **161**, 254 (1985).
- ²⁴ P. W. Brouwer, *Phys. Rev. B* **51**, 16878 (1995).
- ²⁵ P. W. Brouwer, *Phys. Rev. B* **63**, 121303 (2001).
- ²⁶ C. W. J. Beenakker, *Rev. Mod. Phys.* **69**, 731 (1997).
- ²⁷ M. Switkes, Ph. D. thesis (Stanford, 1999).
- ²⁸ Note that Eq. (A2) only fixes Ψ up to right-multiplication with a unitary matrix (orthogonal matrix in the presence of time-reversal symmetry). However, this unitary (orthogonal) matrix can be absorbed into H_1 and H_2 , the distribution of which is invariant under unitary (orthogonal) transformations.
- ²⁹ J.N.H.J. Cremers, Ph.D. Thesis, Harvard University, in preparation.
- ³⁰ K. Zyczkowski and M. Kus, *Phys. Rev. E* **53**, 319 (1996).
- ³¹ E. Brézin, S. Hikami, and A. Zee, *Nucl. Phys. B* **464**, 411 (1996).